University of Szeged

Faculty of Pharmacy

Institute of Pharmacodynamics and Biopharmacy

Evaluating the *in vitro* anticancer potential of natural products and repurposed drugs in human cancer cell lines with different HPV status

Summary of Ph.D. Thesis

Hiba Faroug Muddather Abdallah

Szeged, Hungary

2025

University of Szeged, Faculty of Pharmacy
Doctoral School of Pharmaceutical Sciences
Pharmacodynamics, Biopharmacy and Clinical Pharmacy Program
Head of the program: Prof. Dr. István Zupkó, D.Sc.

Institute of Pharmacodynamics and Biopharmacy

Supervisors: Prof. Dr. István Zupkó, D.Sc.

Dr. Zsuzsanna Schelz, Ph.D.

Evaluating the *in vitro* anticancer potential of natural products and repurposed drugs in human cancer cell lines with different HPV status

Summary of Ph.D. Thesis

Hiba Faroug Muddather Abdallah, MPharm

Complex Exam Committee:

Chairman: Prof. Dr. István Szatmári
Members: Prof. Dr. Zsuzsanna Helyes
Dr. Anita Sztojkov-Ivanov

Defense Board:
Chairman: Prof. Dr. István Ilisz
Reviewers: Dr. Mónika Csontné Kiricsi
Dr. Ana Sofia Fernandes Martins
Secretary: Dr. Gábor Katona
Members: Dr. Zita Zalán

Szeged, Hungary
2025

Introduction

Cancer is the second leading cause of death globally, with nearly 19.96 million new cases and 9.74 million deaths reported in 2022, including non-melanoma skin cancers. Its growing burden is attributed to population aging, lifestyle factors, and environmental changes, particularly in developing countries where cancer data and healthcare access are limited.

Cervical cancer remains one of the leading causes of cancer-related deaths among women, especially in low- and middle-income countries. In 2022, it caused about 660,000 new cases and 350,000 deaths, with nearly 85% occurring in developing regions where the mortality rate is 18 times higher than that in high-income countries. HPV infection has been identified as a necessary cause, particularly types 16 and 18, which account for about 70% of cases. Early detection and HPV vaccination significantly reduce the disease burden.

Head and neck (HN) cancer accounts for about 890,000 new cases and 450,000 deaths each year, making it the sixth most common cancer worldwide. Approximately 90% are squamous cell carcinomas (SCC) originating from epithelial tissues of the oral cavity, pharynx, and larynx, with tobacco and alcohol responsible for 72% of cases. The incidence varies greatly by region, being highest in Southeast Asia due to areca nut use and rising in Western countries due to HPV-related oropharyngeal cancer. By 2030, the number of HNSCC cases is expected to increase by 30%, with most of these cases likely being HPV-related.

Peganum harmala L. (*P. harmala*), a perennial plant native to the Middle East, North Africa, and Central Asia, has been traditionally used to treat various diseases. It contains alkaloids such as harmine, a β-carboline derivative with multiple biological effects, including cytotoxic and antitumor activities against breast, ovarian, thyroid, bladder, gastric cancers, melanoma, and leukemia.

Drug repurposing, which involves using approved drugs for new medical purposes, reduces development time and costs while improving safety outcomes. Examples of repurposed drugs include retinoic acid, zoledronic acid, and thalidomide. Statins, through inhibition of 3-hydroxy-3-methylglutaryl coenzyme-A (HMG-CoA) reductase and the mevalonate pathway, interfere with cell proliferation and survival, showing antineoplastic potential in various cancers. Levosimendan, a calcium sensitizer and phosphodiesterase (PDE) III inhibitor used for heart failure, exhibits

vasodilatory, antiarrhythmic, and nitric oxide (NO)-mediated effects, making it a potential candidate for repositioning in oncology due to its multifaceted pharmacological actions.

2. Study aims and objectives

The current study investigated selected substances' potential antiproliferative and antimetastatic properties on a panel of adherent breast, gynecological, and oral squamous cell carcinoma cell lines. Furthermore, it aimed to unveil the underlying mechanism of action of the most promising agents.

The specific objectives of the performed studies are outlined as follows:

- Evaluating the growth-inhibitory potential of the tested agents against selected adherent human cancer cell lines and subsequently determining the IC_{50} values of the most promising compounds using a standard MTT assay.
- Assessing tumor selectivity by comparing the growth-inhibitory effects of the tested agents on cancerous cells to non-cancerous fibroblast cell lines.
- Determining the capacity of the compounds to induce apoptotic morphological cell alterations and changes in cell membrane integrity using Hoechst 33258–propidium iodide (HOPI) fluorescent double staining.
- Exploring the influence of the tested compounds on cell cycle progression by measuring the cellular DNA content using a flow cytometer.
- Investigating the pro-apoptotic effect using the fluorimetric quantification of caspase-3 enzymatic action.
- Measuring mitochondrial membrane potential through JC-10 staining.
- Evaluating the influence of the tested compound on microtubule dynamics using a tubulin polymerization assay.
- Exploring the antimetastatic properties by investigating the effects of the substances on cell migration and invasion using wound healing and Boyden chamber assays, respectively.

3. Materials and methods

3.1. Plant and chemicals

Colleagues from the Institute of Pharmacognosy, University of Szeged, Hungary, extracted and isolated the *P. harmala* samples. Atorvastatin and rosuvastatin were acquired from Gedeon Richter Plc. (Budapest, Hungary). Meanwhile, levosimendan was obtained from Merck Life Science Ltd. (Budapest, Hungary). Stock solutions of the tested substances were prepared in dimethyl sulfoxide (DMSO). All experimental reagents and kits were procured from Merck Life Science Ltd. (Budapest, Hungary) unless specified otherwise. The cell culture media were purchased from Capricorn Scientific GmbH (Ebsdorfergrund, Germany), while the media supplements were obtained from Lonza Group Ltd. (Basel, Switzerland).

3.2. Cell lines and culture

The adherent cell lines were obtained from the European Collection of Authenticated Cell Cultures (ECACC, Salisbury, UK), except for SiHa and C33A (American Type Culture Collection, Manassas, VA, USA). Oral squamous cell carcinoma cells were obtained from DSMZ – German Collection of Microorganisms and Cell Cultures GmbH (Braunschweig, Germany). The non-cancerous human fibroblast cell line (MRC-5) was provided by Professor Mónika Kiricsi (University of Szeged, Hungary). Cells were cultured under standard conditions in appropriate growth media containing essential supplements.

3.3. Antiproliferative assay

A colorimetric MTT assay was carried out to determine the growth-inhibitory properties of the investigated agents. The cell controls were incubated only in the medium, while cisplatin (Ebewe Pharma GmbH, Unterach, Austria) was used as a positive control. After 72 h of incubation in cell culture conditions, absorbance values were determined using a microplate reader, and data from six-point dose-response curves were fitted by GraphPad Prism 5.01 or 9.01. Each experiment was performed twice, each with five replicates.

3.4. Hoechst 33258–propidium iodide fluorescent double staining

The apoptotic morphological effects of the tested compounds were examined using fluorescent double staining. Cells were stained with lipophilic Hoechst 33258 (5 μg/ml, HO) and hydrophilic propidium iodide (3 μg/ml, PI). After replacing the medium in the wells, imaging was performed with a Nikon Eclipse TS100 fluorescence microscope supplied with filters appropriate for detecting HO and PI fluorescence.

3.5. Flow cytometry

Cells were analyzed by flow cytometry to determine their DNA content using a CytoFLEX-V0-B4-RO flow cytometer or FACSCalibur flow cytometer. The obtained data were evaluated using ModFit LT 3.3.11 or Kaluza Analysis software. The sub-G1 phase identified apoptotic cells. Moreover, Annexin V–Alexa 488 (AnnV)–PI dual fluorescent staining was carried out to evaluate the apoptotic rate. Events were recorded by FACSCalibur flow cytometer, and the obtained data were processed using CellQuest software.

3.6. Determination of caspase-3 activity

Caspase-3 activity was measured using a fluorimetric assay kit (CASP3F). The fluorescence intensity of the cleaved substrate, which is directly proportional to the amount of active caspase-3, was measured by a CLARIOstarPlus reader, at which fluorescence was recorded at 360 nm excitation and 460 nm emission. Cisplatin was the positive control.

3.7. Determination of mitochondrial membrane potential

To assess alterations in mitochondrial membrane potential, we utilized a microplate-based JC-10 assay. Fluorescence was recorded using a microplate reader, detecting green signals at 490 nm excitation/525 nm emission and red signals at 540 nm excitation/590 nm emission. The membrane potential was expressed as the ratio of red (healthy) to green (apoptotic) fluorescence.

3.8. Tubulin polymerization assay

Tubulin polymerization was tested using a commercially available cell-free assay kit (Cytoskeleton Inc., Denver, CO, USA). Paclitaxel served as a positive control. Absorbance was recorded every minute for 60 min. The highest difference between six absorbance values at two consecutive time intervals was considered as the maximum rate of tubulin polymerization (Vmax).

3.9. Antimigratory assay

To assess the influence of the tested substances on cell motility, a wound healing assay was conducted using a specific silicone insert (ibidi GmbH, Gräfelfing, Germany). The percentage of cell migration was calculated based on the images captured at 0, 24, and 48 h and analyzed with ImageJ software.

3.10. Boyden chamber assay

Cell invasion was measured using Matrigel-coated Boyden chambers. Images per chamber were captured using a Nikon Eclipse TS100 fluorescence microscope, and the number of invading cells was quantified using ImageJ software.

3.11. Statistical analysis

Data are presented as mean ± SEM from at least two separate experiments. One-way analysis of variance (ANOVA), followed by Dunnett's test was performed to identify statistical significance using GraphPad Prism 5.01 or 9.0 software for Windows (GraphPad Software, San Diego, CA, USA). *, **, and *** indicate $p < 0.05$, $p < 0.01$, and $p < 0.001$ compared to the controls, respectively.

4. Results

4.1. *Peganum harmala*

4.1.1. Antiproliferative activity and tumor selectivity

Our data showed that the root extract exhibited the highest growth-inhibitory effect among the extracts from other plant parts. On the other hand, harmine exerted a profound growth-inhibitory effect among the purified β-carboline alkaloids (data are not presented). For the tested substances that showed a higher growth-inhibitory effect, IC_{50} values were calculated (Table 1). Furthermore, the results showed no detectable cytotoxicity in NIH/3T3 murine fibroblast cells. Therefore, harmine was selected for further investigations on cervical cancer cells (SiHa) and oral SCC cells (OSCC, UPCI-SCC-154).

Table 1: Calculated IC_{50} values for the most active substances

Cell line	Root	Harmine	Harmol	Cisplatin
	IC_{50} (μM) ± SEM			
HeLa	26.74 ± 3.66	16.56 ± 0.74	>30	12.43 ± 0.15
SiHa	8.47 ± 0.48	6.05 ± 0.52	11.89 ± 2.65	4.80 ± 0.51
C33A	12.95 ± 1.87	12.27 ± 1.65	21.50 ± 0.83	4.70 ± 1.16
MCF-7	9.86 ± 0.67	8.06 ± 1.70	20.50 ± 1.80	8.19 ± 0.14
MDA-MB-231	13.65 ± 0.93	18.77 ± 3.34	>30	19.12 ± 0.02
A2780	4.87 ± 1.09	6.54 ± 0.17	13.40 ± 0.83	1.34 ± 0.04
UPCI-SCC-154	10.83 ± 0.88	13.30 ± 0.57	22.59 ± 0.24	1.29 ± 0.001
UPCI-SCC-131	23.13 ± 2.30	27.85 ± 0.50	>30	1.37 ± 0.15
NIH/3T3	56.43 ± 0.32	>30	>30	5.11 ± 0.38

4.1.2. Harmine-induced cell cycle disturbances

Our results revealed that in SiHa cells, harmine induced cell cycle arrest at the S and G2/M phases 48 h and 72 h post-incubation, in a dose-responsive manner (Figure 1A). Moreover, the sub-G1 population was increased, particularly after a longer incubation of 72 h. Under consistent

experimental conditions, UPCI-SCC-154 showed concentration-dependent G2/M cell cycle arrest and S phase reduction 48 h after harmine exposure. Longer incubation (72 h) led to a concentration-dependent accumulation of cells at sub-G1, with a significant reduction in the cell population at the G1 phase (Figure 1B).

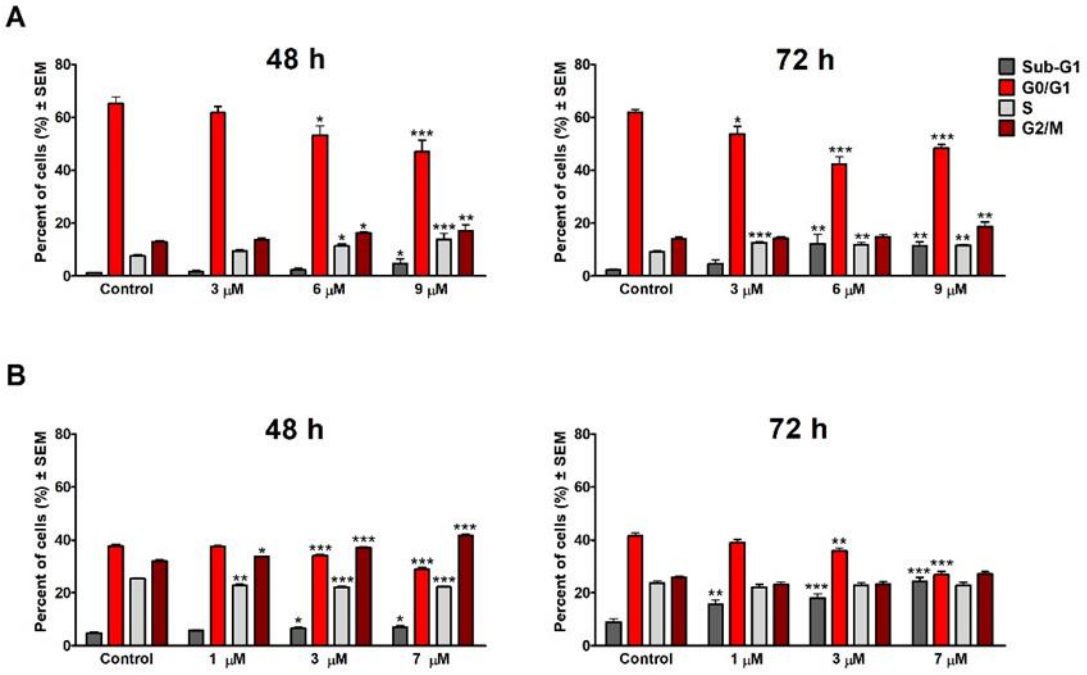

Figure 1. Effect of harmine on the cell cycle distribution after treatment with different compound concentrations tested for 48 and 72 h on HPV-positive cervical cancer cells SiHa **(A)** and HPV-positive OSCC cells UPCI-SCC-154 **(B)**. Results are expressed as mean values ± SEM of the data from two independent experiments performed in triplicate samples.

4.1.3. Apoptosis induction

Visualized chromatin condensation and nuclear fragmentation indicated early apoptosis in the SiHa and UPCI-SCC-154 cells treated with harmine for 24 h (images not shown). Additionally, late apoptosis or necrosis was evident due to penetration of propidium iodide, suggesting possible disruption of cell membrane integrity.

The pro-apoptotic effect of harmine was further investigated employing an Ann V–Alexa 488–PI flow cytometric apoptosis detection kit. Our results revealed that after 24 h of treatment of the SiHa cells with harmine, the percentage of apoptotic cells increased from 7.1 to 13.8% in a dose-dependent manner (Figure 2).

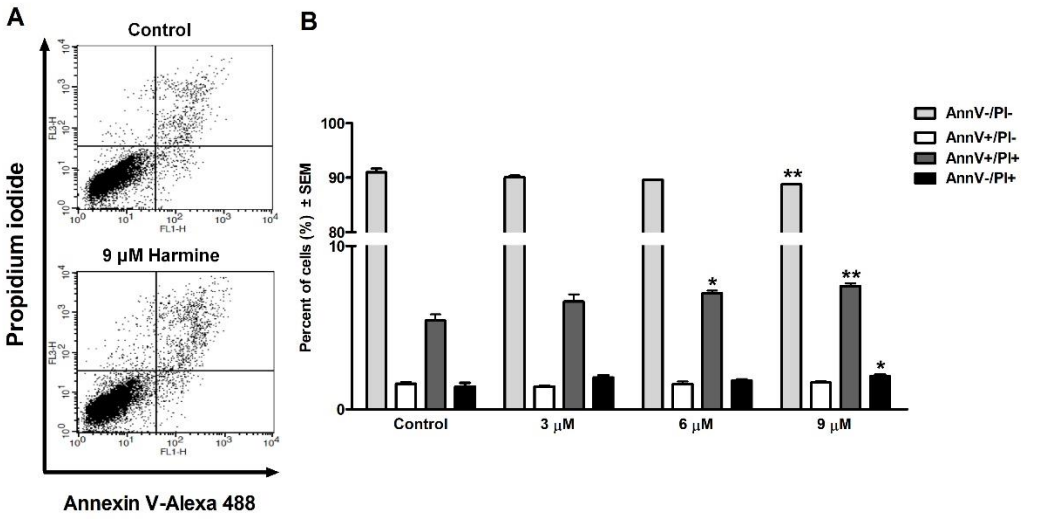

Figure 2. Harmine-induced late apoptosis in SiHa cells after 24 h of incubation. Representative dot plots **(A)** and the percentage of apoptotic cells **(B)** were quantified and distinguished using cell staining with AnnV–Alexa 488–PI. The numbers of viable (AnnV-/PI-), early apoptotic (AnnV+/PI-), late apoptotic (AnnV+/PI+), and necrotic (AnnV-/PI+) populations are given as percentages. Data are presented as mean ± SEM.

4.1.4. Determination of harmine-induced caspase-3 activity

72 h after harmine treatment, a significant increase in caspase-3 enzyme activity in both tested cell lines was detected (Figure 3).

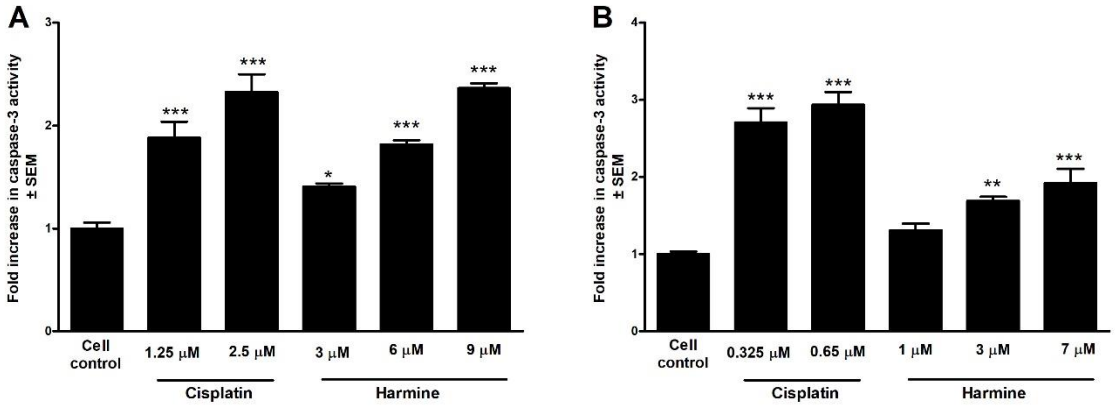

Figure 3. Caspase-3 activity measurement after 72 h harmine exposure on cervical cancer cells SiHa **(A)** and OSCC cells UPCI-SCC-154 **(B)**. Results are presented as mean values ± SEM of the data from two independent experiments performed in triplicate.

4.1.5. Effects of harmine on tubulin polymerization

A standard cell-independent tubulin polymerization assay was performed to evaluate the effect of harmine on microtubule polymerization. As directed by the manufacturer, paclitaxel was used as

the positive control. The highest applied concentration of harmine (150 µM) significantly increased the extent and rate (Vmax) of tubulin polymerization, relative to the control (Figure 4).

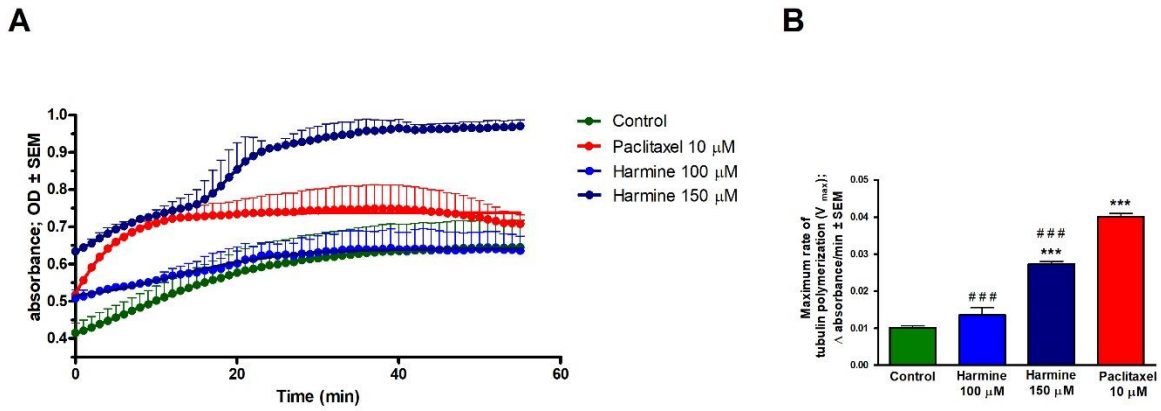

Figure 4. Harmine augments tubulin polymerization using a cell-independent tubulin polymerization assay. The tubulin was incubated with the general tubulin buffer and paclitaxel as negative and positive controls, respectively. **(A)** Tubulin polymerization curve plotted using GraphPad Prism 5.01 software. **(B)** Maximum rate of tubulin polymerization. Each condition was performed in duplicate at a minimum of two separate measurements. Data presented as mean ± SEM, ### indicates $p < 0.001$ compared to paclitaxel.

4.1.6. Antimigratory effects of *P. harmala* root extract and harmine

Cervical HPV 16-positive SiHa and HPV-negative C33A cells, as well as the HPV 16-positive OSCC cell line UPCI-SCC-154, were utilized to demonstrate the impact of different concentrations of the root extract and harmine on cell migration. The investigated substances significantly inhibited the migration capacity of the mentioned cells, even at sub-inhibitory concentrations (Figures 5 and 6).

4.1.7. Anti-invasive effects of harmine

Harmine reduced the invasive capacity of the investigated cancer cell lines, compared to the controls. In the cervical cancer cells SiHa, the effect was markedly detected 24 h post-harmine incubation; however, in the case of the OSCC cells UPCI-SCC-154, a dose-dependent effect was detected after a prolonged incubation period of 48 h (Figure 7).

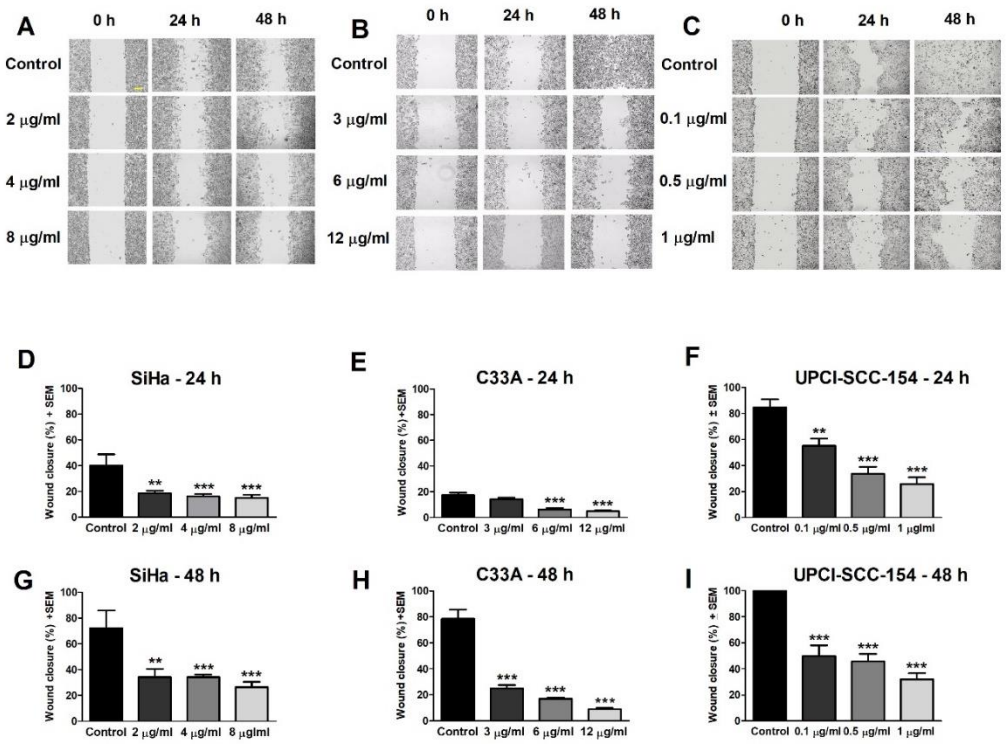

Figure 5. Effect of root extract on cell migration. Representative images of wound closure at 0, 24, and 48 h post-treatment for HPV-positive cervical cancer cells SiHa **(A)**, HPV-negative cervical cancer cells C33A **(B)**, and HPV-positive OSCC UPCI-SCC-154 cells **(C)**. The bar in the photos indicates 100 µm. Graphs indicate the percentage of cell migration at 24 and 48 h post-treatment of SiHa cells **(D, G)**, C33A cells **(E, H)**, and UPCI-SCC-154 cells **(F, I)**, relative to the controls. Results are presented as mean values ± SEM of data from at least two independent measurements, each performed in triplicate.

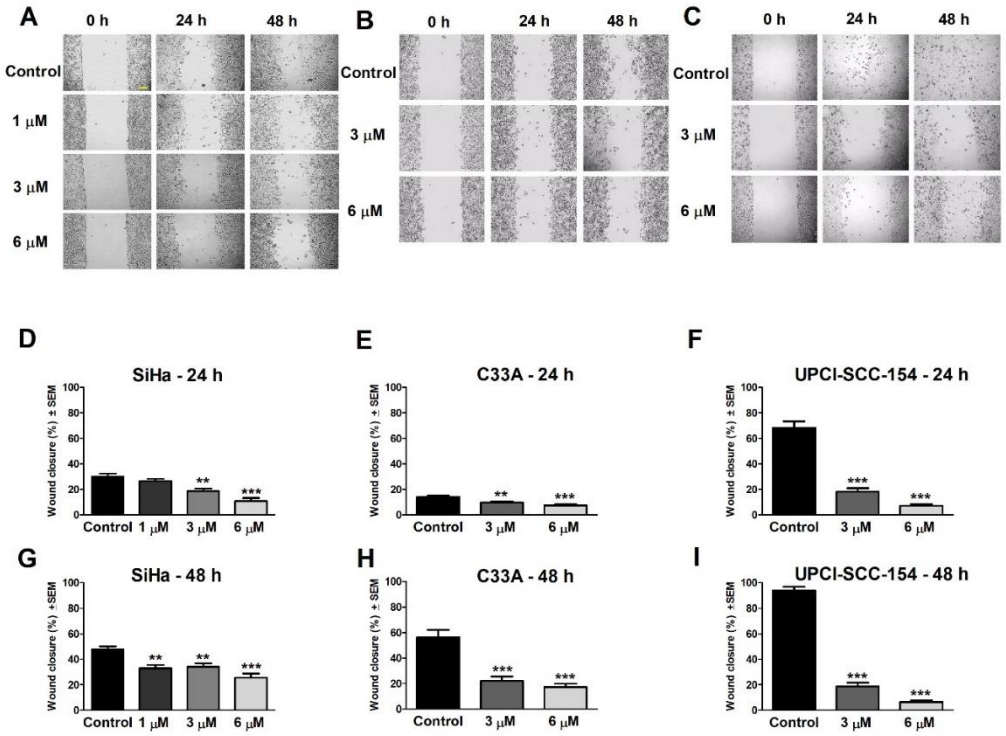

Figure 6. Effect of harmine on cell migration. Representative images of wound closure at 0, 24, and 48 h post-treatment for HPV-positive cervical cancer cells SiHa **(A)**, HPV-negative cervical cancer cells C33A **(B)**, and HPV-positive OSCC UPCI-SCC-154 cells **(C)**. The bar in the photos indicates 100 µm. Graphs indicate the percentage of cell migration at 24 and 48 h post-treatment of SiHa cells **(D, G)**, C33A cells **(E, H)**, and UPCI-SCC-154 cells **(F, I)**, relative to the controls. Results are presented as mean values ± SEM of data from at least two independent measurements, each performed in triplicate.

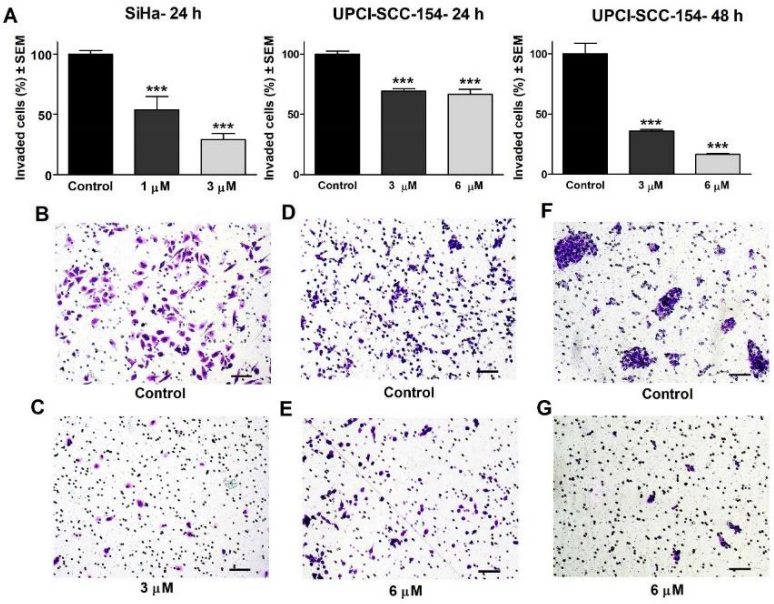

Figure 7. Effect of harmine on the invasiveness of investigated cancer cell lines. The percentage of invading cells after harmine treatment at specified intervals **(A)**. The anti-invasive potential of the test compound is illustrated by representative images: control **(B)** and 3 µM harmine **(C)** of SiHa, 24 h post-treatment; and controls after 24 h **(D)** and 48 h **(F)**, 6 µM harmine incubated for 24 h **(E)** and 48 h **(G)** in OSCC cells UPCI-SCC-154. The bar in the photos indicates 100 µm. Results are expressed as mean values ± SEM of data from two independent measurements with duplicate samples.

4.2. Statins

4.2.1. Antiproliferative activity and tumor selectivity

The growth-inhibitory effects of atorvastatin and rosuvastatin were evaluated in selected cancer cell lines, revealing that the lipophilic atorvastatin exerted higher antiproliferative activity than the hydrophilic rosuvastatin (Table 2). Based on its lower IC_{50} values and the limited existing data on its anticancer mechanisms, atorvastatin was chosen for further *in vitro* investigation on HPV-negative C33A and HPV16-positive UPCI-SCC-154 cells. Both statins exhibited reduced cytotoxicity toward non-cancerous MRC-5 fibroblast cells, indicating tumor selectivity.

Table 2. Growth-inhibitory effects of atorvastatin and rosuvastatin on the cell lines tested

Cell line	Atorvastatin	Rosuvastatin	Cisplatin
	IC_{50} (μM) ± SEM		
MCF-7	61.01 ± 2.63	> 100	8.19 ± 0.14
T47-D	8.32 ± 1.07	> 100	18.36 ± 0.88
MDA-MB-231	2.57 ± 0.21	18.22 ± 0.79	19.12 ± 0.02
HeLa	20.27 ± 0.52	64.91 ± 1.27	12.43 ± 0.15
SiHa	12.02 ± 1.72	38.39 ± 0.22	4.80 ± 0.51
C33A	4.61 ± 0.11	31.63 ± 0.56	4.70 ± 1.16
A2780	4.02 ± 0.56	96.13 ± 0.51	1.34 ± 0.04
UPCI-SCC-154	9.21 ± 0.97	94.09 ± 0.61	1.29 ± 0.001
UPCI-SCC-131	34.74 ± 1.15	94.16 ± 1.28	1.37 ± 0.15
MRC-5	48.64 ± 2.29	> 100	4.74 ± 0.23

4.2.2. Atorvastatin-induced cell cycle disturbances

Atorvastatin induced cell cycle disruption in both C33A and OSCC cells. In C33A cells, it caused G2/M arrest and increased sub-G1 populations (Figure 8A), while in OSCC cells, it led to G1 accumulation, S phase reduction, and elevated sub-G1 fractions, with its effects intensifying after 48 h (Figure 8B).

4.2.3. Apoptosis-inducing effect visualized by fluorescent double staining

Pronounced alterations were visualized in cell morphology and membrane integrity after exposing UPCI-SCC-154 cells to various concentrations of atorvastatin. Fluorescence images revealed an increase in cells emitting intense blue fluorescence, indicating early apoptosis. In addition,

especially after prolonged incubation, there was a rise in the proportion of cells emitting red fluorescence, suggesting secondary necrosis (images not shown).

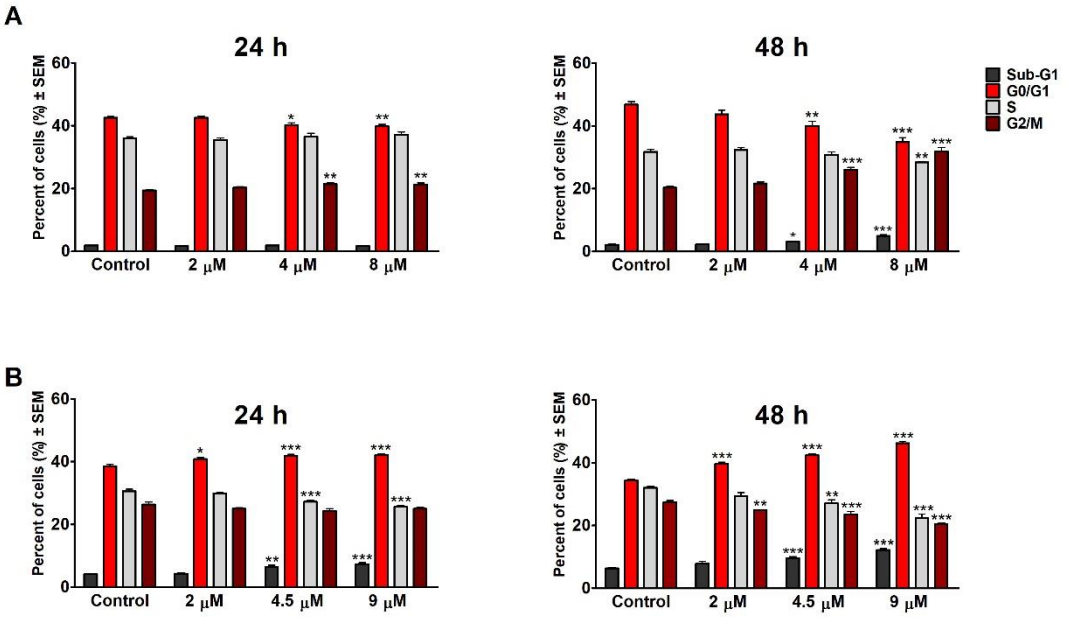

Figure 8. Effect of atorvastatin on the cell cycle distribution after treatment with different compound concentrations tested for 24 and 48 h on HPV-negative cervical cancer cells C33A **(A)** and HPV-positive OSCC cells UPCI-SCC-154 **(B)**. Results are expressed as mean values ± SEM of the data from two independent experiments performed in triplicate samples.

4.2.4. Determination of atorvastatin-induced caspase-3 activity

After 48 h of exposing OSCC cells to varying concentrations of atorvastatin, our findings revealed a dose-dependent increase in caspase-3 activity, with comparable effects to the utilized positive control (cisplatin), as shown in Figure 9.

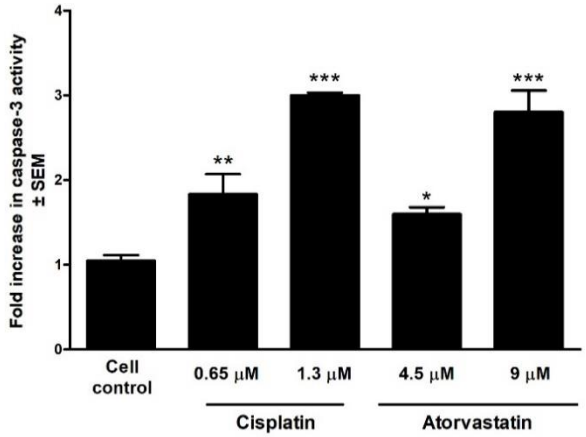

Figure 9. Caspase-3 activity measurement after 48 h of atorvastatin exposure on UPCI-SCC-154 cells. Results are presented as mean values ± SEM of the data from two independent experiments performed in triplicate.

4.2.5. Atorvastatin-induced mitochondrial membrane damage

Using the JC-10 assay kit, atorvastatin induced a concentration-dependent elevation of mitochondrial membrane depolarization. Hydrogen peroxide and cisplatin were used as positive controls (Figure 10).

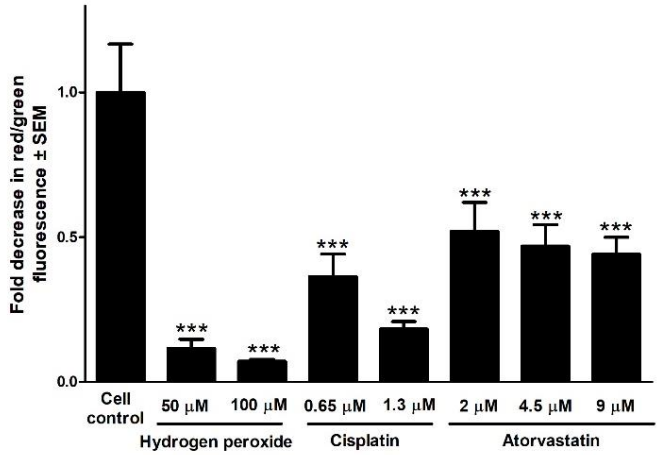

Figure 10. Mitochondrial membrane potential of UPCI-SCC-154 cells after 48 h exposure to atorvastatin using JC-10 staining. Results are expressed as mean values ± SEM of the data from three independent experiments.

4.2.6. Antimigratory effects of atorvastatin

Atorvastatin exhibited concentration- and time-dependent antimigratory effects assessed 24 and 48 h post-treatment. Consistent patterns were detected in the C33A and UPCI-SCC-154 cell lines (Figure 11).

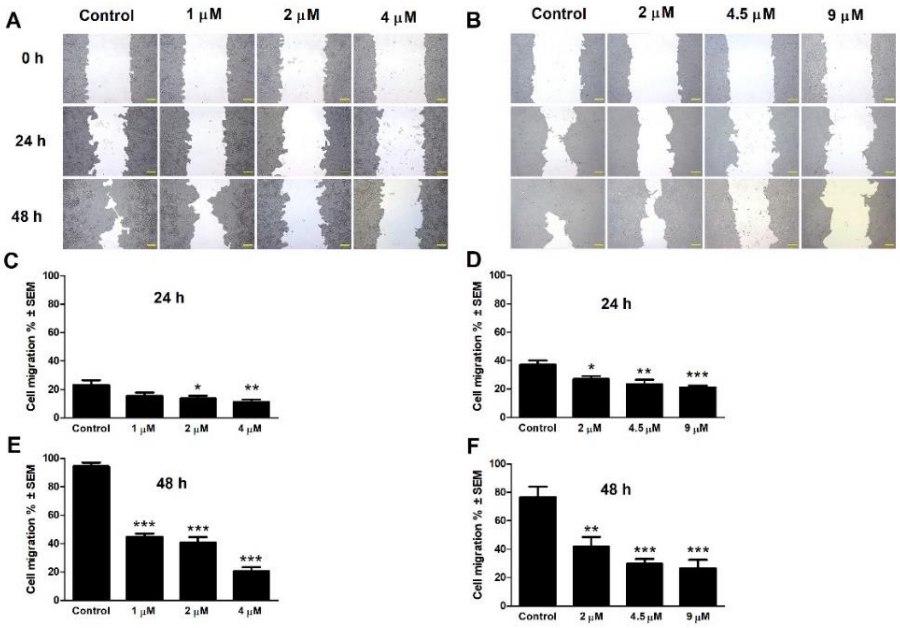

Figure 11. Effect of atorvastatin on cell migration. Representative images of wound closure at 0, 24, and 48 h post-treatment for C33A cells **(A)** and UPCI-SCC-154 cells **(B)**. The bar in the photos indicates 100 μm. Graphs indicate the percentage of cell migration for C33A cells **(C, E)** and UPCI-SCC-154 cells **(D, F)**, relative to the controls. Results are presented as mean values ± SEM of the data from two independent measurements with triplicate.

4.2.7. Anti-invasive effects of atorvastatin

The invasion assay revealed that atorvastatin markedly reduced the invasive capacity of cancer cells in a concentration- and time-dependent manner. C33A cells showed a noticeable, dose-dependent decline in the number of invaded cells after 48 h, whereas OSCC cells exhibited modest inhibition at 24 h and a pronounced reduction after 48 h of treatment (Figure 12).

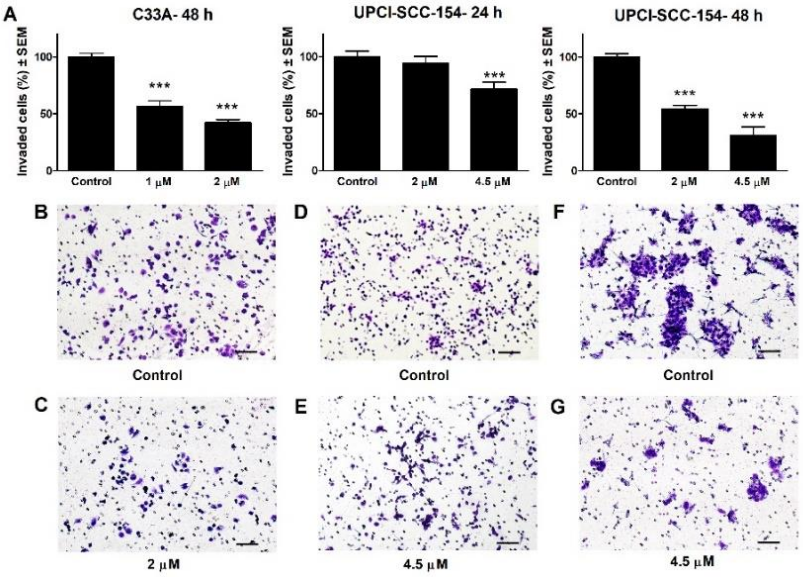

Figure 12. Effect of atorvastatin on cancer cell invasion. The percentage of invading cells after atorvastatin treatment **(A)**. The anti-invasive potential of the test compound is illustrated by representative images: control **(B)** and 2 μM atorvastatin **(C)** of C33A, 48 h post-treatment; and controls after 24 h **(D)** and 48 h **(F)**, 4.5 μM atorvastatin, incubated for 24 h **(E)** and 48 h **(G)** on UPCI-SCC-154 cells. The bar in the photos indicates 100 μm. Results are expressed as mean values ± SEM of the data from two independent measurements with duplicates.

4.3. Levosimendan

4.3.1. Antiproliferative activity and tumor selectivity

Levosimendan showed the strongest antiproliferative effect against HPV-negative C33A cells (IC_{50} = 58.42 μM), while showing limited activity in SiHa and HeLa cells. Despite being less potent than cisplatin, it demonstrated selectivity toward C33A over non-cancerous MRC-5 cells. Accordingly, the C33A cell line was selected for subsequent experiments (Table 3).

Table 3. Antiproliferative effects of levosimendan on human cervical cancer cell lines

Cell line	Levosimendan	Cisplatin
	IC_{50} (μM) [95% CI (μM)]	
SiHa	128.80 [109.30–148.20]	4.29 [3.72–4.95]
HeLa	170.00 [144.50–195.50]	12.14 [10.18–14.46]
C33A	58.42 [45.75–71.08]	5.85 [5.37–6.38]
MRC-5	315.70 [304.70–326.70]	4.96 [3.51–6.99]

CI: confidence interval.

4.3.2. Levosimendan-induced cell cycle disturbances

Our findings demonstrated a notable disruption of cell cycle progression, observed 24 h following levosimendan exposure. 48 h post-exposure, a significant increase in hypodiploid sub-G1 cell populations was recorded (Figure 13).

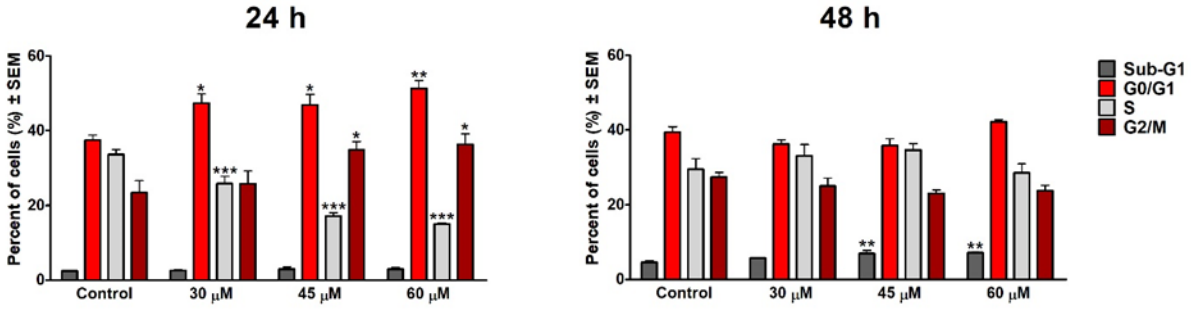

Figure 13. Effect of levosimendan on the cell cycle distribution after treatment with different concentrations of the compound tested for 24 and 48 h on HPV-negative cervical cancer cells C33A. Results are expressed as mean values ± SEM of the data from two independent experiments performed in triplicate.

4.3.3. Apoptosis-inducing effect visualized by fluorescent double staining

To observe the cellular morphological changes in C33A cells following levosimendan treatment, HOPI double staining was conducted 24 h and 48 h after levosimendan incubation. Early apoptotic and necrotic cells were visualized (images not shown).

4.3.4. Antimigratory effects of levosimendan

Levosimendan inhibited C33A cell migration significantly at 60 µM after 24 h of treatment, with more profound, dose-dependent effects observed after 48 h (Figure 14).

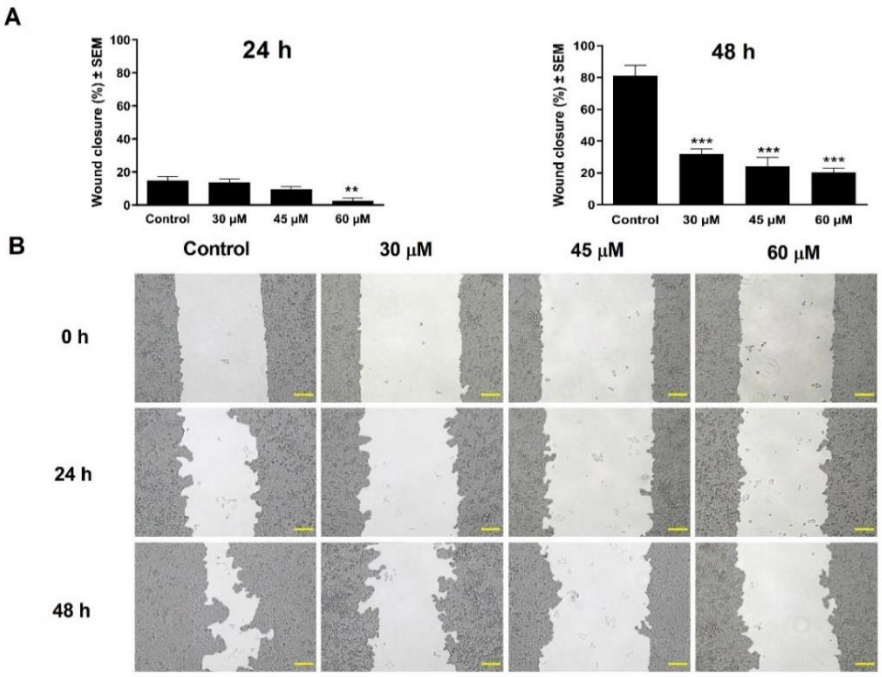

Figure 14. Effect of levosimendan on C33A cell migration. Graphs display the percentage of cell-free areas following cell treatment compared to the untreated controls **(A)**. Representative images illustrate the inhibition of wound closure at 0, 24, and 48 h post-treatment **(B)**. The bar in the pictures indicates 100 μm. Data are expressed as mean ± SEM. The findings are based on the results of two independent experiments performed in triplicate.

4.3.5. Anti-invasive effects of levosimendan

48 h post-levosimendan incubation, the number of invaded cancer cells was profoundly reduced in a concentration-based manner (Figure 15).

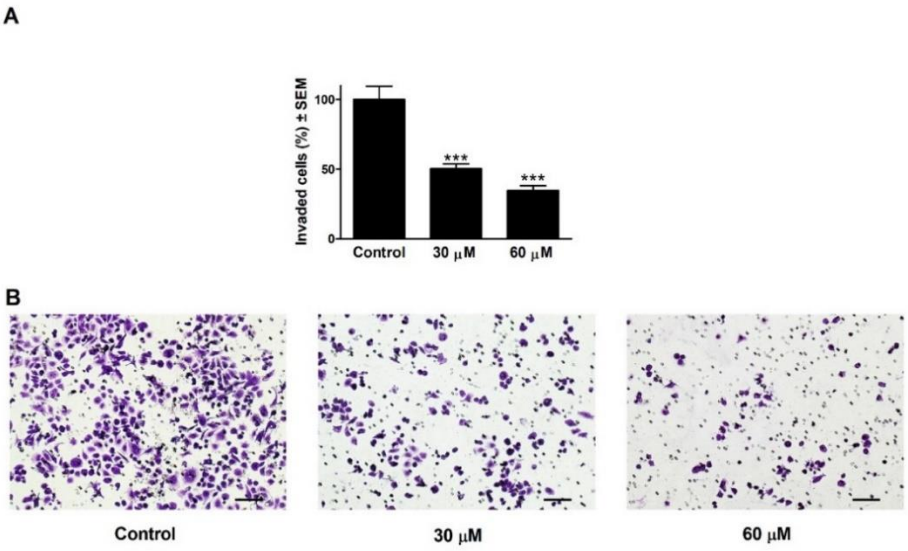

Figure 15. Effect of levosimendan on the invasiveness of C33A. The percentage of invading C33A cells after 48 h of levosimendan treatment (**A**). Representative images at 48 h post-treatment (**B**). The bar in the pictures indicates 100 μm. Data are presented as mean ± SEM of two independent experiments performed in duplicate.

5. Discussion

5.1. Anticancer potential of *Peganum harmala*

The role of natural compounds and their derivatives in cancer research continues to grow, offering a broad chemical basis for developing new therapies. Many natural alkaloids, including vinca alkaloids and camptothecin, are effectively used as antineoplastic agents. Harmine, a β-carboline

alkaloid, has traditionally been recognized for its potential anticancer activity, and previous studies have confirmed its antitumor properties across different cancer types. However, to our knowledge, no study has thoroughly examined the mechanism of harmine in cervical and HN cancers.

The present study investigated the antineoplastic effects of *P. harmala* crude extract and its isolated alkaloids across multiple human adherent cancer cell lines. The results revealed that the root extract exhibited the highest growth-inhibitory effect, while harmine emerged as the most potent isolated β-carboline alkaloid. Harmine selectively inhibited cancer cell proliferation without affecting non-cancerous murine fibroblast (NIH/3T3) cells. Based on these findings, the HPV-16–positive cervical cancer (SiHa) and OSCC (UPCI-SCC-154) cell lines were selected for further mechanistic studies.

Based on multiple *in vitro* investigations, including cell cycle analyses, HOPI double staining, AnnV–Alexa488 and PI dual staining, and measurement of caspase-3 activity, harmine showed antiproliferative activity and apoptosis-inducing capability. Within 24 h of treatment, HOPI staining revealed that harmine efficiently induced characteristic apoptotic features, such as chromatin condensation, membrane blebbing, DNA fragmentation, and PI uptake, in a dose-dependent manner. Furthermore, AnnV–Alexa488–PI flow cytometry analysis showed a marked increase in late apoptotic (AnnV+/PI+) cell population after 24 h of exposure to harmine, alongside a rise in sub-G1 phase populations, which represent apoptotic cells. The activation of caspase-3, a crucial executioner cysteine protease enzyme, was significantly elevated in both cervical and OSCC cells treated with harmine, confirming the involvement of caspase-dependent apoptosis in harmine's anticancer mechanism.

Cell cycle analyses in SiHa cells after 48 and 72 h of harmine exposure revealed a significant arrest at the S and G2/M phases with G1 depletion. The effect was concentration-dependent, exhibiting pronounced arrest at 9 µM after 48 h and minimal changes at 6 µM. After 72 h, these changes became more evident. In contrast, HPV-positive OSCC cells showed higher sensitivity, with G2/M arrest and S phase depletion at concentrations as low as 1 µM after 48 h. Prolonged exposure led to sub-G1 accumulation, confirming apoptosis induction. These findings align with previous studies showing harmine-induced G2/M arrest in human umbilical vein endothelial cells (HUVEC), hepatocellular, and colon cancer cells, although G1 arrest was reported in some leukemic and melanoma cell lines, indicating cell line-specific effects. Notably, the harmine

concentrations used in our antiproliferative assay (1–30 μM) are relatively high compared to reported human plasma levels. Limited pharmacokinetic data indicate that human plasma concentrations remain below 10 μM post-intravenous administration and decline rapidly. Therefore, the 1–9 μM range used in our mechanistic assays is closer to physiologically achievable levels, whereas higher doses may have limited clinical relevance and potential safety concerns.

Furthermore, harmine enhanced microtubule formation and tubulin assembly in a concentration-dependent manner, although to a lesser extent than paclitaxel, a known microtubule stabilizer.

To assess the antimetastatic potential of *P. harmala*, wound-healing and Boyden chamber assays were performed. In the wound-healing assay, harmine significantly reduced wound closure in SiHa, C33A, and UPCI-SCC-154 cells in a dose-dependent manner. The same results could be detected in the *P. harmala* root extract-treated cells. In the Boyden chamber assay, harmine decreased invading cell numbers in both SiHa and UPCI-SCC-154 cell lines proportionally to applied concentrations. These findings support harmine's ability to inhibit cell motility and invasion, supporting its antimetastatic activity. Given that microtubule dynamics are essential for cancer cell migration and invasion, disrupting tubulin function can limit metastatic progression. Thus, the observed effects of the compound may partly result from its ability to interfere with tubulin polymerization.

In conclusion, our findings demonstrated harmine's capability to reduce cancer cell proliferation, promote apoptosis, and disturb cell cycle progression in HPV-positive cervical cancer and OSCC cells, likely by stabilizing microtubule polymerization. Additionally, it exhibited substantial antimigratory and anti-invasive effects.

5.2. Antitumor activity of statins

Despite progress in drug development, the effectiveness of the currently available treatments remains limited, and the FDA approval rate of new drugs has markedly declined since the 1990s. This growing demand for more potent antineoplastic agents has attracted attention to drug repurposing as a promising alternative approach.

Statins inhibit HMG-CoA reductase in the hepatic mevalonate pathway, thereby reducing cholesterol synthesis. Studies have shown that statins can exert antineoplastic effects through both mevalonate-dependent and independent mechanisms. Although statins have demonstrated activity

across several cancer types, their effects on cervical and OSCC cells remain insufficiently explored, warranting further investigation. Therefore, the current study evaluated the antiproliferative effects of two statins, atorvastatin and rosuvastatin, across several human cancer cell lines. Atorvastatin showed higher potency, achieving significant growth inhibition at lower concentrations (lowest IC_{50} = 2.57 μM) and displaying activity comparable to cisplatin. Both compounds were tested on non-cancerous MRC-5 fibroblasts to assess selectivity. Although experimental concentrations exceeded those used in standard therapy, similar plasma levels can be reached with high-dose statin regimens, and localized delivery strategies may enhance therapeutic relevance.

Based on tumor selectivity and specificity findings, HPV-negative cervical (C33A) and HPV-positive OSCC (UPCI-SCC-154) cell lines were selected for further investigations. Cell cycle analysis revealed that atorvastatin induced G2/M arrest in C33A cells and G0/G1 arrest with S phase suppression in OSCC cells. Extended exposure (48 h) led to more alterations and increased the sub-G1 population, indicating apoptosis induction, which was more pronounced in OSCC.

In addition to the apoptosis detected via the flow cytometer and the visualized cellular morphological changes, a marked reduction in mitochondrial membrane potential was detected, indicating that mitochondrial dysfunction contributes to atorvastatin-induced apoptosis. In line with this mechanism, increased caspase-3 activity was evident in UPCI-SCC-154 cells post 48 h of atorvastatin treatment.

Atorvastatin also demonstrated potent antimetastatic effects. In wound-healing and Boyden chamber assays, it significantly inhibited migration and invasion in both cell lines in a dose- and time-dependent manner, even at sub-inhibitory concentrations.

Overall, our results showed the promising antiproliferative and antimetastatic effects of atorvastatin on HPV-negative cervical cancer cells C33A and HPV-positive OSCC cells UPCI-SCC-154. The compound triggered cellular apoptosis through the activation of the caspase-3 enzyme. Moreover, it exerted substantial cell cycle disturbances as well as pronounced antimigratory and anti-invasive effects.

5.3. Antineoplastic properties of levosimendan

Levosimendan, initially approved for managing decompensated severe chronic heart failure, has gained interest as a potential anticancer agent due to its diverse pharmacological properties and established safety profile. Limited studies have demonstrated its *in vitro* antitumor activity, with hematopoietic lymphoma cells showing high sensitivity. Moreover, levosimendan synergized with 5-fluorouracil (5-FU) in treated bladder cancer cells.

This study investigated levosimendan's anticancer activity and potential mechanism against three cervical carcinoma cell lines with distinct HPV statuses (SiHa, HeLa, and C33A). Levosimendan demonstrated higher specificity toward HPV-negative C33A cells, with an IC_{50} value of 58.42 µM, suggesting its potential as an adjuvant agent to suppress tumor proliferation. The compound also exhibited a higher IC_{50} value in non-cancerous MRC-5 cells, indicating tumor selectivity. Furthermore, levosimendan induced apoptosis in C33A cells, as evidenced by morphological changes observed by fluorescent staining, and increased sub-G1 cell populations after 48 h of treatment.

Previous studies have shown that NO can inhibit cancer cell proliferation and induce cell cycle arrest. Levosimendan enhances NO production in endothelial cells through activation of signaling pathways involving p38 mitogen-activated protein kinases (MAPKs), extracellular signal-regulated kinase (ERK), and protein kinase B (PKB/Akt). Our results showed that levosimendan disrupted cell cycle progression in C33A cells, increasing the G1 phase population, suppressing S phase, and inducing modest G2/M arrest after 24 h incubation. At the same time, a significant rise in sub-G1 apoptotic populations was recorded after 48 h.

Levosimendan and its active metabolite, OR-1896, are potent PDE III inhibitors, an enzyme that plays a role in breaking down cAMP. Since cAMP elevation can inhibit cancer cell migration, levosimendan might consequently attenuate tumor metastasis. In the current study, the compound significantly reduced C33A cell migration and invasion in a concentration- and time-dependent manner. Collectively, these findings demonstrate that levosimendan exerts antiproliferative, pro-apoptotic, cell cycle-disruptive, and antimetastatic effects against HPV-negative cervical cancer C33A cells.

LIST OF PUBLICATIONS RELATED TO THE THESIS

I. **Muddather, H.F.,** Nasibova, T., Szebeni, G.J., Gémes, N., Bózsity, N., Minorics, R., Garayev, E., Orhan, I.O., Herbette, G., Schelz, Z., Hohmann, J., Zupkó, I. Potential Anticancer Effects of *Peganum harmala* in Human Papillomavirus-Related Cervical and Head and Neck Cancer Cells. *Front. Pharmacol*. 2025, 16:1668827. https://doi.org/10.3389/fphar.2025.1668827. IF: 4.8 / Q1.

II. **Muddather, H.F.**, Bózsity, N., Balogh, B.T., Schelz, Z., Zupkó, I. *In Vitro* Investigation of the Antiproliferative and Antimetastatic Effects of Atorvastatin: A Focus on Cervical and Head and Neck Cancers. *Pharmaceutics*. 2025, 17: 1253. https://doi.org/10.3390/pharmaceutics17101253. IF: 5.5 / D1.

III. Schelz, Z., **Muddather, H.F.**, Jaski, F.S., Bózsity, N., Zupkó, I. An *In Vitro* Investigation of the Antiproliferative and Antimetastatic Effects of Levosimendan: Potential Drug Repurposing for Cervical Cancer. *Curr. Issues Mol. Biol.* 2024, 46: 6566–6579. https://doi.org/10.3390/cimb46070391. IF: 3 / Q2.

PRESENTATIONS AND POSTERS RELATED TO THE THESIS

I. **Muddather, H.F.,** Nasibova, T., Szebeni, G.J., Gémes, N., Bózsity, N., Minorics, R., Schelz, Z., Hohmann, J., Zupkó, I. Anticancer Potential of *Peganum harmala*: Inhibition of Proliferation and Metastasis in Human Cancer Cell Lines, XXVIII. Spring Wind Conference, 2025, Budapest, Hungary. Oral presentation.

II. **Muddather, H.F.**, Bózsity, N., Balogh, B.T., Schelz, Z., Zupkó, I. Investigating Antitumor Properties of HMG-CoA Reductase Inhibitors on Human Cancer Cells *in Vitro*. 1st International Health Science Conference, 2025, Szeged, Hungary. Poster presentation.

III. **Muddather, H.F.**, Balogh, B.T., Bózsity, N., Schelz, Z., Zupkó, I. Antineoplastic Effects of Atorvastatin and Rosuvastatin on Human Cancer Cells, Fiatal Gyógyszerkutatók Fóruman, 2024, Budapest, Hungary. Oral presentation.

IV. **Muddather, H.F.**, Balogh, B.T., Bózsity, N., Schelz, Z., Zupkó, I. *In Vitro* Investigation of Antiproliferative and Antimetastatic Effects of Atorvastatin and Rosuvastatin. EUGLOH Annual Summit 2024, Szeged, Hungary. Poster presentation.

V. **Muddather, H.F.**, Balogh, B.T., Bózsity, N., Schelz, Z., Zupkó, I. Antiproliferative and Antimetastatic Effects of Atorvastatin and Rosuvastatin on Human Cancer Cells. Congressus Pharmaceuticus Hungaricus XVII and EUFEPS Annual Meeting 2024, Debrecen, Hungary. Poster presentation.

VI. **Muddather, H.F.,** Nasibova, T. *In Vitro* Investigation of *Peganum harmala* on Human Cancer Cell Lines, XV. Clauder Otto Conference, 2023, Budapest, Hungary. Oral presentation.

VII. **Muddather, H.F.,** Schelz, Z., Nasibova, T., Hohmann, J., Zupkó, I. *In Vitro* antiproliferative and antimetastatic properties of *Peganum harmala*, XXVI. Spring Wind Conference, 2023, Miskolc, Hungary. Oral presentation.

VIII. **Muddather, H.F.,** Schelz, Z., Nasibova, T., Hohmann, J., Zupkó, I. *In Vitro* antiproliferative and antimetastatic properties of *Peganum harmala*, 4th International Conference on Pharmaceutical and Medical Sciences, 2022, Martin, Slovakia. Online oral presentation.